ASIAN JOURNAL OF PHARMACEUTICAL AND CLINICAL RESEARCH

INNOVARE ACADEMIC SCIENCES
Knowledge to Innovation

Vol 18, Issue 12, 2025

Online - 2455-3891
Print - 0974-2441

Research Article

ENHANCED WOUND HEALING USING ANTHOCYANIN-LOADED SILK SERICIN/POLYVINYL ALCOHOL NANOFIBERS: A BIOMATERIAL-BASED APPROACH

JAJNADATTA PANDA[1]*, ABHISEK PAL[1], PRITIPADMA PANDA[2], ARCHANA PANIGRAHY[1]

[1]Department of School of Pharmaceutical Sciences, Siksha "O" Anusandhan (Deemed to be University), Bhubaneswar, Odisha, India.
[2]KIIT School of Pharmacy, KIIT (Deemed to be University), Bhubaneswar, Odisha, India.
*Corresponding author: Jajnadatta Panda; Email: jajnadattapanda414@gmail.com

Received: 14 August 2025, Revised and Accepted: 13 October 2025

ABSTRACT

Objective: The goal of this study was to create a nanofibrous wound dressing using silk sericin (SS) and polyvinyl alcohol (PVA) that included anthocyanin (ACN) phytoconstituents in different amounts to promote wound healing, pH monitoring, and antibacterial activity.

Methods: PVA–SS–ACN nanofibers were created by electrospinning with varying concentrations of solution (A1, A4, and A5), yielding average fiber diameters of 144.13 nm, 169.15 nm, and 192.51 nm, respectively. Up to 85 h of continuous herbal ingredient release was demonstrated by the nanofibers' bead-free shape. Through structural and thermal characterizations using scanning electron microscopy, Fourier transform infrared, and thermogravimetric analysis, the stability of the nanofibrous mats up to 50°C, the chemical integration of ACNs, and the creation of smooth fibers were all confirmed.

Results: The most potent antibacterial action against *Staphylococcus aureus* and *Escherichia coli* was shown by the nanofibrous mat loaded with 0.1 and 1% w/w ACN. In this study, the comparison between 0.1 and 1% the therapeutic efficacy is higher in 1% because the dose of the drug increased. Histological and *in vivo* wound healing investigations demonstrated superior healing efficiency, reduced acute and chronic inflammation, and accelerated tissue regeneration compared to untreated control groups.

Conclusion: The PVA–SS–CAN nanofibrous dressing's remarkable antibacterial, anti-inflammatory, and controlled drug-release qualities make it a promising option for advanced wound healing applications. The interwoven network of fibers also aids in exudate control, reducing the discomfort of dressing changes by absorbing excess fluid and preventing the dressing from adhering to the wound.

Keywords: Electrospinning nanofiber, Wound healing, Silk sericin, Anthocyanin.

 DOI: http://dx.doi.org/10.22159/ajpcr.2025v18i12.56522. Journal homepage: https://innovareacademics.in/journals/index.php/ajpcr

INTRODUCTION

Any disruption in the structural or functional continuity of living tissue brought on by physical, chemical, microbiological, thermal, or immunological damage is referred to as a wound. Haemostasis, inflammation, proliferation, and remodelling are the processes that contribute to healing; however, infection risks and environmental factors, including aging, stress, smoking, alcohol consumption, and environmental conditions, can hinder successful skin regeneration and result in chronic wounds or scarring [1]. The focus of current research is on environmentally sustainable practices and effective healing, with particular attention on biodegradable biomaterials and environmentally friendly production techniques [2]. In this area, natural biofilm-forming agents are showing promise. Pharmaceutical nanotechnology offers advantages over traditional dosage forms by enabling targeted distribution of active pharmaceutical ingredients (APIs) with enhanced absorption distribution metabolism excretion (ADME) profiles and controlled release [3]. There are several types of nano-formulations, such as electrospun nanofibers, nanogels, liposomes, and nanoparticles. Because it can create nanofibers with high surface area, porosity, and three-dimensional structures that are appropriate for drug loading, electrospinning has particular promise for wound healing [4]. These methods, which have different applications and problems, include side-by-side electrospinning, coaxial, modified coaxial, and mono-axial electrospinning. Multifunctional drug delivery is made possible by core-shell and Janus structures, which improve therapeutic and bactericidal properties [5]. As matrices for biomedical and cosmetic applications, such as skin therapies, anti-aging products, and wound dressings, both natural and synthetic polymers are being investigated. Because of its hydrophilic amino acid makeup, which allows for strong water retention and the maintenance of a moist wound environment necessary for quick tissue repair, silk sericin (SS), a natural silk protein generated from Bombyx mori cocoons, plays a critical role in wound healing [6]. Accelerated granulation and re-epithelialization are the results of its support for extracellular matrix remodeling, collagen deposition, and fibroblast and keratinocyte proliferation. Along with its anti-inflammatory activities that inhibit pro-inflammatory cytokines and prevent chronic inflammation, sericin also possesses antioxidant qualities that shield tissues from oxidative damage [7]. Its potential for wound healing is further enhanced by its biocompatibility, biodegradability, and capacity to function as a barrier against microbial invasion [8]. Conversely, anthocyanins (ACNs), which are naturally occurring flavonoid pigments present in fruits and vegetables, provide a substantial contribution due to their potent anti-inflammatory, antibacterial, and antioxidant qualities. In order to lower the risk of infection, they neutralize reactive oxygen species, suppress inflammatory mediators, and have bactericidal action against both Gram-positive (Staphylococcus aureus) and Gram-negative (Escherichia coli) pathogens [9]. Furthermore, anthocyanins shield fibroblasts and keratinocytes from early senescence, encourage angiogenesis for improved oxygen and nutrition delivery, and boost collagen synthesis [10]. One special benefit of anthocyanins is that they change colour in response to pH, which makes them ideal for smart wound dressings because it enables visual monitoring of wound conditions [11]. Sericin and anthocyanins work in concert in electrospun PVA nanofibers; sericin promotes cell division and keeps the fibers hydrated, while anthocyanins have pH-sensitive, antioxidant, and antibacterial properties. When combined, they form a multipurpose bioactive

scaffold that has the potential to improve wound care applications by promoting wound status monitoring, decreasing infection, faster healing, and reducing inflammation [12].

EXPERIMENTAL METHODS AND MATERIALS

ACN phytoconstituents powder obtained from Vinayak Ingredients (INDIA) Pvt. Ltd. Silk sericin phytoconstituents powder obtained from Silklon Ventures, Bangalore, Karnataka (INDIA) Pvt. Ltd. PVA obtained from Loba Chemie (INDIA) Pvt. Ltd. Sodium carbonate, sodium hydrogen carbonate, disodium hydrogen phosphate, potassium dihydrogen phosphate, and sodium chloride obtained from COTEX CHEM Pvt. Ltd. Wistar rats are treated from SPS, SOA, Deemed to be University.

Preparation of stock solutions for electrospinning technology

PVA (10% w/v) was dissolved in deionized water after being agitated for 24 h. Simultaneously, the sericin solution was heated in water to 80°C and agitated for 2 h using a magnetic stirrer to concentrate it to 5% w/v [13]. ACN vegetable phytoconstituents containing the total mass of dissolved polymers and various concentrations of various phytoconstituents (0.00, 0.1, and 1.0% w/v) were added to the mixture and mixed for 24 h at room temperature before electrospinning. The elements utilized to make nanofibers are explained in detail in Table 1 and Fig. 1. The ACN solution was then mixed with the prepared PVA and sericin solutions at various concentrations, and the resultant mixtures were electrospun to form a nanofibrous matrix.

The electrospinning procedure was carried out at room temperature and standard atmospheric pressure, with the spun nanofibers vacuum-dried at room temperature for 48 h [14].

Process of electrospun nanofiber

A 5 mL syringe with a metal needle was filled with the prepared solution and connected to a syringe pump. The critical parameters of the electrospun nanofiber applied voltage of 18 kV, the needle gauge 21, needle flow rate 1.5 mL/h, a revolving collector drum at ~1000 rpm, temperature 35°C, and tip-to-collector distance: 13 cm, 40% relative humidity. The nanofiber coated in aluminum foil, the polymer was released from the syringe tip and deposited as nanofibers on the collector. Nanofibers were produced using two methods: high voltage or varied distances from the syringe to a revolving drum. These nanofibers were later employed throughout the experiment [15].

Morphological analysis

Observation of the electrospun deposition's morphologies was carried out using a scanning electron microscope (SIGMA Field Emission Scanning Electron Microscope from CARL ZEISS). The scanning electron microscopy (SEM) photographs provided data for measuring the average nanofiber diameters and their distributions. The electrospun nanofiber surfaces were examined in detail using field emission-SEM (FE-SEM) images taken with a Zeiss Supra 40VP apparatus. A platinum-palladium coating, approximately 3.0 nm in thickness, was applied to

Table 1: The different formulations and their ratios

Formulations	Polyvinyl alcohol 10% w/v (mL)	Sericin 5% w/v (mL)	Deionized water	Final conc. of anthocyanin phytoconstituents (%)	Final volume
A	2.00	2.00	q. s	0.00	05 mL
B	2.00	2.00	q. s	0.1	05 mL
C	2.00	2.00	q. s	1.0	05 mL

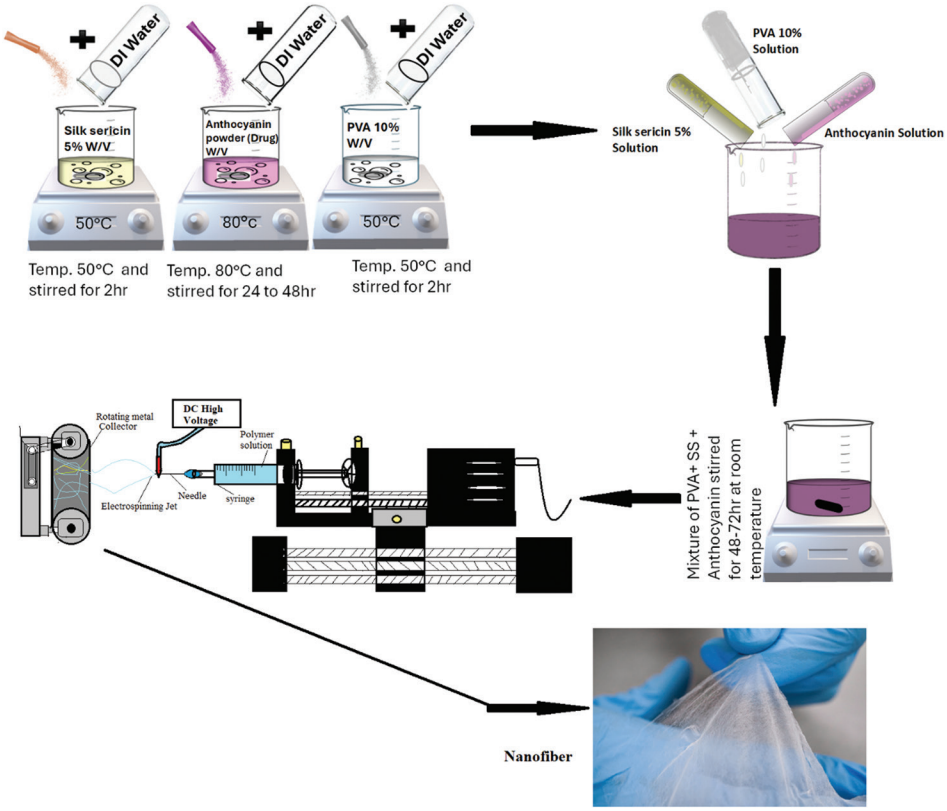

Fig. 1: Schematic representation of the nanofiber's preparation

the sample surfaces to enable SEM imaging [16].

Physico-chemical characterization of nanofiber

The Fourier transform infrared (FTIR) spectra of pure PVA/SS and PVA/SS/ACN composite fibers were analyzed using an FTIR spectrometer (Alpha-E, Bruker, Billerica, MA, USA) equipped with a zinc selenide crystal. Measurements were performed in attenuated total reflectance mode within the wavenumber range of 4000–600 cm^{-1} [17].

Differential scanning calorimetry (DSC)/thermal activity

To investigate the thermal properties of typical fiber samples, a DSC (200 F3 DSC, Maia, Netzsch, Selb, Germany) was used. Aluminum pans with perforated lids were used to cut and securely seal a small quantity of the selected fibers (about 2 mg). The reference was a hermetically sealed aluminum pan with a perforated lid. The environment used for the study was nitrogen gas. The film temperature was gradually increased from 0°C to 400°C to produce the heating curve. The samples were kept for 5 min after they reached 400°C before chilling to 0°C. For the duration of the experiment, the thermal scanning rate was kept at 10°C/min [18].

Antimicrobial activity

The effects of antimicrobial for the control mixture of solution (without the drug [PVA-SS]), sericin, PVA, and ACN solution were investigated against 2 model organisms, *S. aureus* (Gram +ve) and *E. coli* (Gram −ve), utilizing the disc diffusion method. In this experiment, the solutions were split into discs measuring 15 mm in diameter. A 200 µL aliquot of each bacterial strain (1×10^6 CFU/mL) was cultured on a cotton swab and was evenly distributed across the solidified nutrient agar. The 10 µL of drug solution-loaded discs were then positioned on the agar surfaces that had been inoculated. To reduce the risk of dehydration, the plates were wrapped with parafilm and kept at 37°C for 24 h. After incubation, the zones of inhibition around the discs were measured [19].

Swelling study

The swelling proportion of electro-spun nanofibers was established through the procedure of submerging 0.1 g of nanofibers in a solution consisting of 50 mL of phosphate-buffered saline (PBS, pH 7.4) [20]. This immersion was carried out under controlled conditions, both at cooling and room temperature for 24 h, allowing the nanofibers to reach their maximum swelling equilibrium. Subsequently, the swelling ratio was computed using a specific equation denoted as Eq. (1).

The percentage swelling was computed using the equation below:

$$\text{Percentage Swelling } (\%) = \frac{W_a - W_i}{W_i} \times 100 \quad (1)$$

Where W_a is the sample's weight at time t, and W_i refers to its initial weight at the beginning of the experiment.

Drug release pattern of nanofiber

The release behavior of plant phytoconstituent compounds from the samples was thoroughly investigated by immersing the nanofibers (weighing 0.025 g) dissolved in 40 mL of PBS, with a pH of 7.4 at a temperature of 37°C over a period ranging from 0 to 360 h. To regulate the amount of released plant phytoconstituent compounds, an ultraviolet (UV)-spectrophotometer (wavelength: 277 nm; Model: 1700, Shimadzu, Japan) was utilized, measuring the amount at the maximum wavelength of 380 nm [19,20]. Measuring by spectrophotometry: The ACN extracts were assessed using spectrophotometry. With a UV-visible spectrophotometer, the absorbance of the finished reaction mixtures was determined at 380 nm. Using the following formula, the sample's % inhibition was determined:

$$\frac{A_{Control} - A_{Sample}}{A_{Control}} \times 100$$

Where $A_{Control}$ represents the absorbance of the control and A_{Sample} denotes the absorbance of the ACN extract.

Statistical analysis

The results were presented as mean±standard deviation, and all measures were carried out in triplicate. The statistical analysis was performed with GraphPad Prism and Microsoft Excel. Linear regression analysis was used to determine the ACN extract's half-maximal inhibitory concentration (IC_{50}) values based on the dose-response data. Statistical significance was determined using a one-way analysis of variance (ANOVA), with $p<0.05$ being deemed statistically significant [21].

***In vivo* wound healing activity**

Wistar rats were chosen, and the weights are in between 180 and 240 g approximately for *in vivo* wound healing assessment. The rats were anesthetized with ketamine hydrochloride, and a standardized wound (such as excisional, incisional, or burn) was induced on their skin through a surgical procedure. One rat received a blank nanofiber composed only of polymers, and the second and third were treated with a nanofiber containing both the drug and polymers. The wound-healing process was monitored throughout the study. Observations were conducted over approximately 21 days. The wound size was measured on the 1st, 14th, and 21st days, and the average wound reduction was calculated [20].

Histological analysis

Wound biopsies were collected on days 10 and 20 of the experiment, including a 2-mm margin of wounded skin, from different animal groups (normal control, stress-induced, standard treatment, and Test-1) following euthanasia [22]. The skin samples were fixed overnight in 10% buffered paraformaldehyde, dehydrated through a graded ethanol series, and embedded in paraffin. Sections of 5 µm thickness were then prepared and stained with hematoxylin and eosin using standard histological procedures. The stained sections were subsequently examined under a light microscope [23,24].

RESULTS AND DISCUSSIONS

Microscopic/morphological analysis

Their droplets are unable to generate high-quality nanofibers in FE-SEM examination because of certain mechanical disturbances. Gravity and capillary breakdown of the spinning jet due to surface tension had an impact on the creation of nanofibers. It was observed that defective nanofibers, including unspun droplets and beads, developed. Table 1 above illustrates PVA-SS and ACN, while Fig. 2 shows the various drug concentrations that were effectively loaded. PVA-SS, PVA-SS-ACN (0.1%), and PVA-SS-ACN (1%) were prepared and evaluated well. The inappropriate viscosity of the spinning solution at low PVA concentrations was the reason for the drop in bead density for PVA-SS-ACN nanofibers as the PVA content rose. The polymer-solvent and polymer-polymer interfaces, conductivity, surface tension, and viscosity are all crucial elements of the electrospinning process. By altering the polymer content, the solution's viscosity may be managed. The orientation of the polymer chain concerning the direction of flow either directly or indirectly, determines the thickness of the polymer solution.

As the shear rate decreases, the orientation of the polymer chain also decreases with the increasing viscosity of the solution. But, as the shear rate increased, the polymer chains became oriented, resulting in a significant decrease in viscosity. Here, both polymers had different viscosity rates, PVA 10% and SS 5% at the shear rate of 10°. The nanofibers are not obtained from SS, obtained from the viscosity of the PVA polymer solution due to the short polymer chain length. All the mixed solutions demonstrated a shear-thinning behavior. Here, (A) means PVA-SS, (B) means PVA-SS-ACN (0.1%), and (C) means PVA-SS-ACN (1%). The mean diameter of the nanofibers generated from A, B, and C solutions was 144.13, 169.15, and 192.51 nm, respectively. Fig. 3 displays the FESEM pictures of spun nanofibers containing altered amounts of the

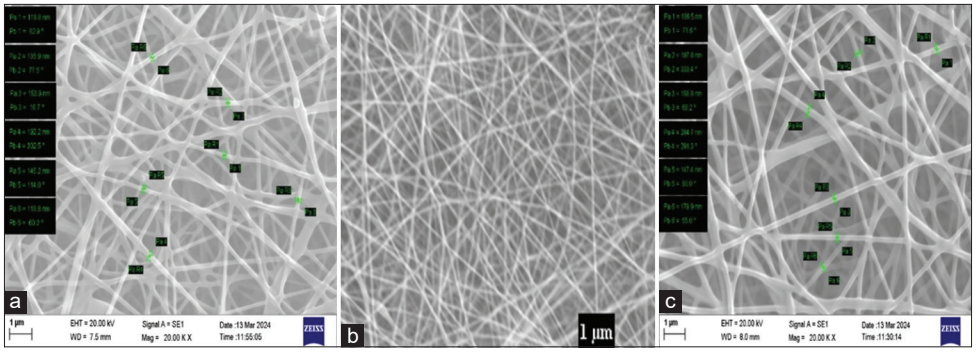

Fig. 2: (a-c) Microscopic structure of nanofibers

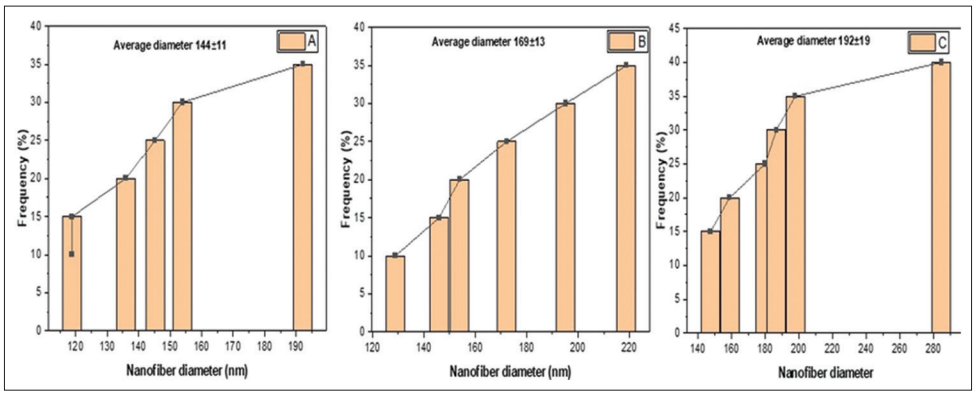

Fig. 3: Bar graph presents the diameter of nanofibers (A, B, and C)

plant-phytoconstituent compound. Table 2 showed the mathematically standard deviation with the average diameter of the nanofiber. It was observed that the morphology of the electrospun nanofibers underwent slight changes after the incorporation of the plant phytoconstituents. The fusion of nanofibers, particularly at their junctions, was noticed and became more evident with a higher phytoconstituent concentration, correspondingly (PVA-SS-ACN ACN=various phytoconstituents concentrations). The increase in nanofiber diameter was attributed to the interaction between the polymer matrix and ACN phytoconstituents, leading to a rise in solution viscosity. The nanofiber diameter expanded with the increasing number of crosslinks in the electrospinning solution. At minimal shear rates, the sample retained energy effectively, maintaining its integrity without distortion. However, as shear rates escalated and neared the yield threshold, the structure gradually deteriorated, ultimately shifting into a liquid state.

When the high voltage and distance values were reduced, the nanofibers' circular cross-sectional morphology changed to a ribbon-like form. Reduced stretching and elongation forces applied to the droplet and liquid jet caused this change, which increased the diameter of the nanofiber. Until the whole solution to the nanofiber is formed at the revolving drum. Before it arrives at the collector, it will not be dried.

FTIR analysis

The FTIR spectrophotometer is a tool utilized for detecting functional groups and analyzing chemical bonds in various compounds. The FTIR spectrum of ACN displays prominent bands at specific wavelengths, which correspond to the characteristic absorption of chemical bonds within the molecule. The absorption band within the wavenumber range of 600–1000 cm^{-1}, referred to as the fingerprint region, indicates the presence of aromatic rings and plays a key role in molecular identification due to its association with distinct vibrational modes unique to each molecule. The band in the FTIR spectrum between 1500 and 2000 cm^{-1} is characteristic of the benzene ring, indicating the presence of C=C, C=N, or C=O bonds. In the FTIR spectrum, the bands between 3600 and 3200 cm^{-1} are characteristic of hydrogen bonds. The absorption bands between 3000 and 2800 cm^{-1} are linked to C–H, O–H, or N–H stretching vibrations. Infrared spectroscopy investigates the elongation and flexion of specific bonds, with the most distinctive bands for differentiating various ionic forms of ACN observed in the 1700–1000 cm^{-1} range, as stronger bonds vibrate faster, particularly those between heavier atoms and lighter ones.

The characteristics of PVA-SS nanofibers after blending and spinning were analyzed using FTIR. The FTIR spectra of PVA, derived from the hydrolysis copolymer of vinyl alcohol and vinyl acetate to form repeat units, exhibit a peak at 2922 cm^{-1}, which is associated with the antisymmetric CH_2 stretching. The peak at 1731 cm^{-1} corresponds to the stretching vibrations of the C=O groups in the residual vinyl acetate repeat units. The Amide I group primarily corresponds to the C=O stretching of the amide group. Minor peaks were observed at 946 cm^{-1}, corresponding to CH_2 rocking, and at 838 cm^{-1}, attributed to C–C stretching. SS, after blending, shows an N–H stretching vibration overlapping with the OH group from serine, with a peak at 3300 cm^{-1}. The Amide II group, exhibiting a peak at 1251 cm^{-1}, is primarily attributed to contributions from N–H bending and C–N stretching. The Amide III group arises from the presence of C–N and C=O stretching.

The absorbance peaks of the ACN pure phytoconstituents at 3270, 2922, and 1725 cm^{-1} correspond to the OH stretching, CH stretching, and C=O stretching vibrations in the pyran ring is typical of flavonoids. Where bands at 1612 cm^{-1} are recognized to the C=C, bands at 1349 and 1147 cm^{-1} correspond to the C–O stretching and C–O–C-stretching, respectively. Minor peaks were raised at 923, 840, 762, and 668 cm^{-1}, indicating C–H deformation-aromatic rings. Therefore, the spectral analysis of the concentrated phytoconstituents shows the presence of O-H, C=O, C=C, and C-O-C functional groups, which are characteristics of ACNs.

Nanofiber scaffold (PVA-SS-ACN) formulation displayed peaks of ACN at 3303, 2923, and 1732cm^{-1}, referring to OH stretching, CH-stretching, and C=O stretching. The peak at 1432 cm^{-1} refers to C–C stretching vibration in the aromatic ring, and stretching in the pyran ring is typical

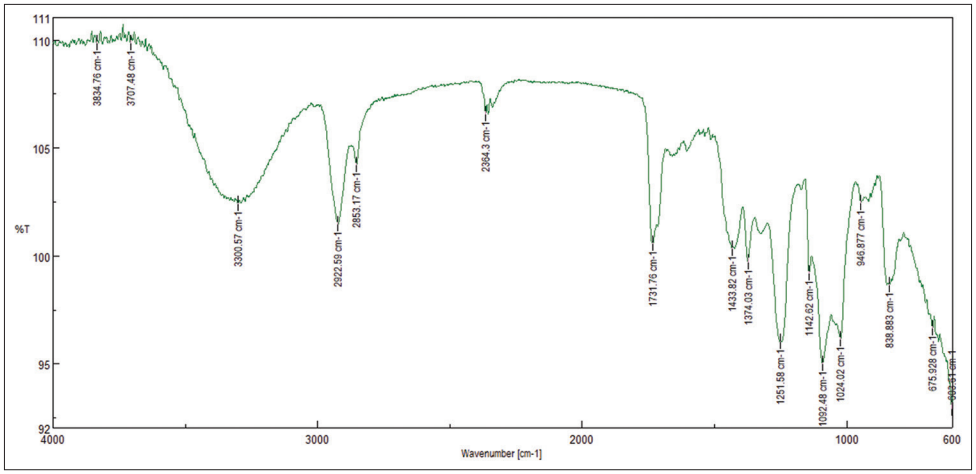

Fig. 4: The Fourier transform infrared graph of A (Control group)

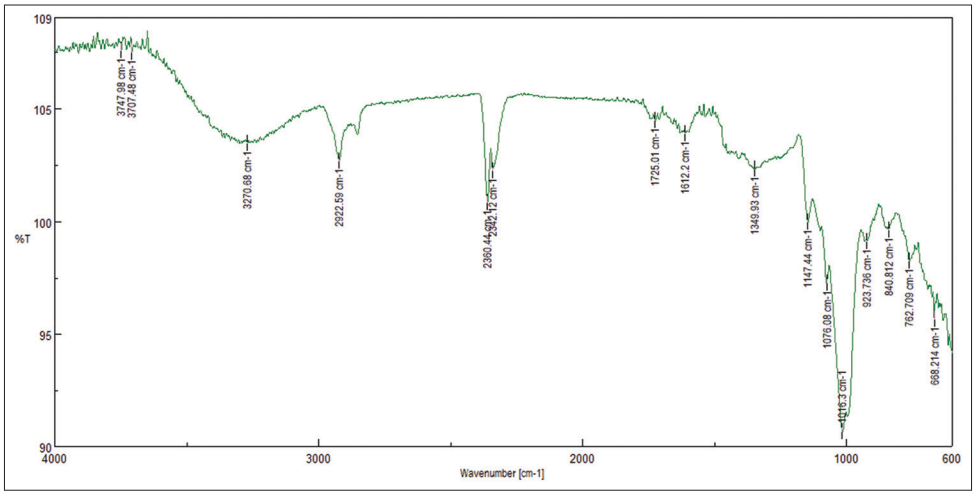

Fig. 5: The Fourier transform infrared graph of B (PVA+SS+ACN 0.1% group). PVA: Polyvinyl alcohol, SS: Silk sericin, ACN: Anthocyanin

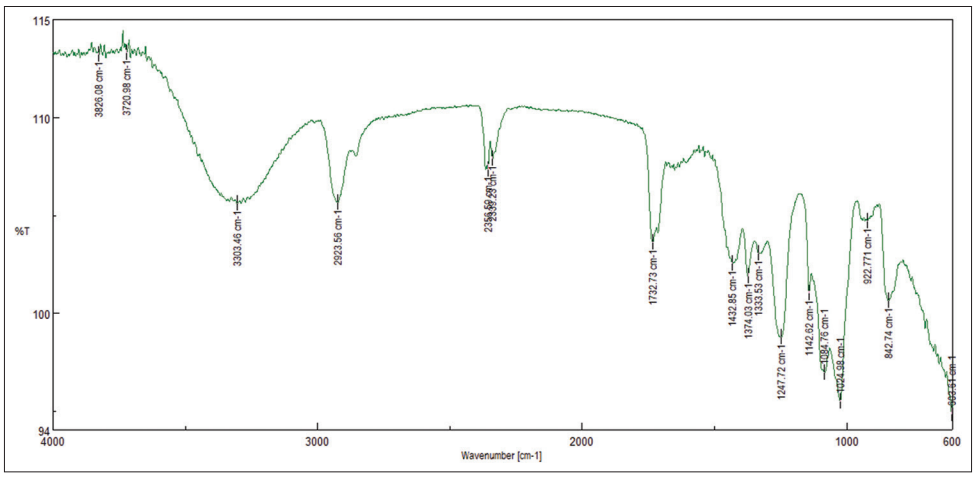

Fig. 6: The Fourier transform infrared graph of C (PVA+SS+ACN 1% group). PVA: Polyvinyl alcohol, SS: Silk sericin, ACN: Anthocyanin

of flavonoids. The peaks at 1247 and 1142cm^{-1} refer to C–O stretching and C–O–C-stretching, respectively. Minor peaks were observed at 922, 842, and 603cm^{-1}, indicating C–H deformation-aromatic rings. Hydrogen bonds in the polypeptide backbone stabilize the secondary structure of proteins, and in the case of sericin, multiple secondary structures lead to overlapping absorptions in the Amide I region, forming a single peak, as shown in Fig. 4, which illustrates the peak fitting results alongside the original FTIR spectrum of the Amide I band. Fig. 5 shows the results of the ACN phytoconstituents. The analysis of the nanofibers after loading with the ACN phytoconstituents is shown in Fig. 6. Figs. 5 and 6 both display the results of the ACN phytoconstituents, with no significant differences observed between the two. These figures examine separate elements of the study, with no direct relationship between the data presented in Figure A and Figures B or C.

Thermal activity (DSC)

The thermal degradation profiles of PVA-SS (without drug), pure ACN phytoconstituents, and PVA-SS-ACN with drug-loaded nanofibrous material were analyzed through TGA to assess the thermal stability of their respective components, as depicted in Fig. 7. The TGA curves of PVA-SS (without drug), pure ACN phytoconstituents, and PVA-SS-ACN with drug-loaded materials exhibited comparable patterns, with the degradation of the materials occurring in three distinct stages of mass loss. The first mass loss occurred between approximately 50–100°C, corresponding to the loss of adsorbed water. The mass losses for both ACN pure phytoconstituents and a mixture of polymer with drug (PVA-SS-ACN) nanofibrous materials were 1%. However, the mass loss of both ACN pure phytoconstituents and PVA-SS-ACN nanofibrous material was slightly lower compared to PVA-SS. This decrease is likely due to the presence of ACN phytoconstituents in the PVA-SS-ACN material, which reduced the amount of adsorbed water in the nanofibrous structure. The second mass losses at 225–265°C against pure ACN phytoconstituents and 220–260°C against PVA-SS-ACN with drug-loaded nanofibrous material as compared to PVA-SS, ACN caused slight decreases (~40°C). The third mass losses at 330–380°C against pure ACN phytoconstituents and 300–350°C against PVA-SS-ACN with drug-loaded nanofibrous material as compared to PVA-SS. The addition of ACN caused slight decreases (~50°C). This study suggests that the phytoconstituents has low thermal stability. TGA examination proved that the addition of ACN to the PVA–SS matrix leads to a decline in thermal stability, which is reflected by the earlier onset of the second thermal degradation phase, indicating temp (~37°C) its suitability for use in wound healing applications at body temperature.

Antimicrobial study

The antibacterial analysis was carried out using the disc diffusion method, a highly effective technique for assessing the antimicrobial properties of SS and ACN compounds, with the results displayed in Fig. 8. The SS and ACN solutions exhibited antibacterial properties, as evidenced by the formation of inhibition zones. In this study, the solution displayed inhibition zones of 19 mm and 23 mm against E. coli and 17 mm and 18 mm against S. aureus, respectively. In contrast, the PVA and PVA-SS solutions showed no inhibition zones and demonstrated no antibacterial activity against S. aureus and E. coli, likely due to the presence of PVA, which lacks inherent antibacterial properties. These findings indicate that both SS and ACN are promising candidates for use in wound dressings.

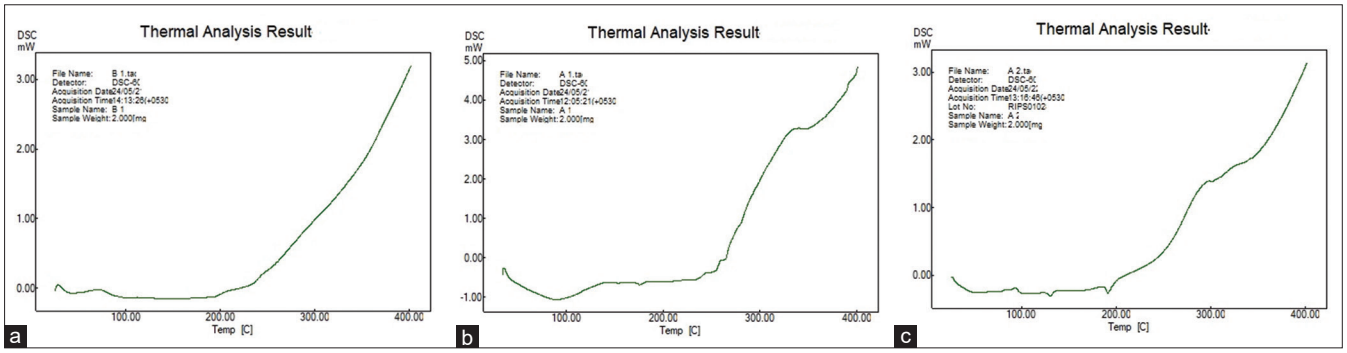

Fig. 7: Thermogravimetric analysis curves represent the data of (a) (PVA+ SS nanofibrous material), (b) pure anthocyanin phytoconstituents, and (c) (PVA-SS-ACN (1%) nanofibrous material). PVA: Polyvinyl alcohol, SS: Silk sericin, ACN: Anthocyanin

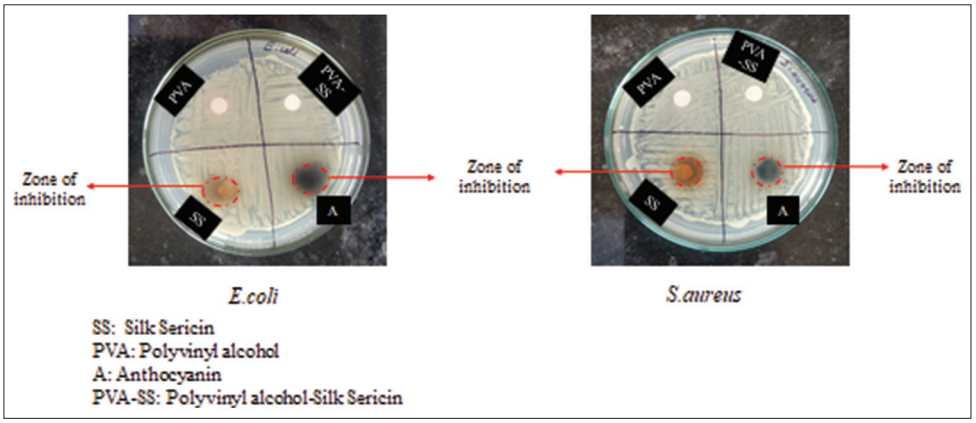

Fig. 8: Antibacterial activity of different nanofiber solutions

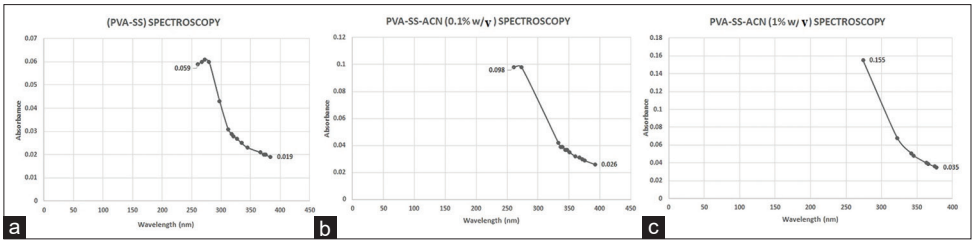

Fig. 9: Drug release profile represents nanofiber of PVA-SS (a), (PVA-SS-[ACN 0.1% w/v])(b), and (PVA-SS-[ACN 1% w/v])(c). PVA: Polyvinyl alcohol, SS: Silk sericin, ACN: Anthocyanin

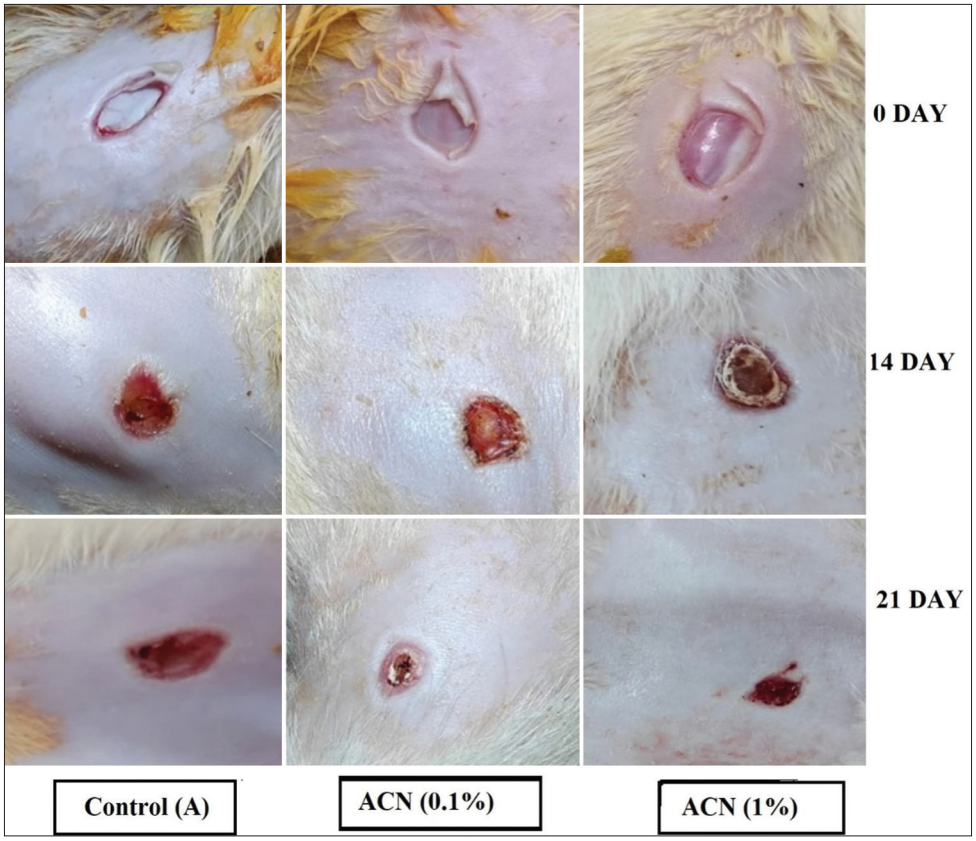

Fig. 10: The wounds from animals in each group were assessed on days 0, 14, and 21 post-treatment

Table 2: Represents the average diameter of nanofibers (A, B, and C)

S. No.	A	B	C
	Diameter	Diameter	Diameter
1	118.8	128.9	186.5
2	135.9	145.9	197.8
3	153.9	153.9	158.8
4	192.2	172.2	284.7
5	145.2	195.2	147.4
6	118.8	218.8	179.9
Mean	144.133	169.15	192.516
Standard deviation	25.027	33.305	44.522

Table 3: Represents the swelling index of anthocyanin-loaded nanofibers

C	Swelling Index (nm)		Percentage
Time	At 4°C	At 27°C	
0 days	15.8	16.1	0
15 days	16.2	16.1	2.53
30 days	16.4	16.1	3.79
45 days	16.7	16.2	5.69
60 days	17.3	16.2	9.44
75 days	17.5	16.2	10.75
90 days	17.7	16.2	12.02

Swelling and Stability activity

The stability of the elevated ACN-loaded nanofibrous material was evaluated over a 3-month period under short-term conditions at both room and refrigerated temperatures (25°C and 4°C), following ICH guidelines, with the results for the swelling index of ACN presented in Table 3.

Table 4: Represents the wound closure (mean±standard deviation) ACN-loaded nanofibers

Group	Day 0	Day 14	Day 21
Control (A1)	0%	42.3±3.1%	65.7±4.5%
ACN (0.1%)	0%	56.8±4.0%	82.5±3.8%
ACN (1%)	0%	68.2±3.5%	92.4±2.7%

n=3, mean±standard deviation, % wound closure of anthocyanin loaded nanofiber., ACN: Anthocyanin

The prepared nanofiber materials showed swelling index values ranging from 15.8 to 17.7 and 2.53% to 12.02%, respectively. Between the analyzed formulations, A5 demonstrated the highest swelling index. As compared to formulations A and B formulations, C swelling facilitates the rapid diffusion of ACNs.

Drug release behavior of nanofiber using UV-spectroscopy

The *in vitro* drug release study for all nanofiber formulations indicated that higher polymer concentrations led to an increased drug release rate. Among the formulations, (C) exhibited the highest drug release, while (B) showed the lowest, as depicted in Fig. 9. Here, we got the result between the wavelengths 250 to 400 nm. As we know previously, the B formulation contains ACN 0.1% w/v and C contains 1% w/v. These findings confirm that the drug release from the formulations was controlled, likely due to the degradation of the nanofibers, which aided in the dispersion of the drug. Sericin is a highly hydrophilic protein due to the presence of numerous polar amino acids, such as serine and aspartic acid, which readily form hydrogen bonds with water molecules. When the PVA–SS matrix comes into contact with moisture, these hydrophilic groups attract and absorb water, causing the material to swell. This swelling increases the mobility and spacing between polymer chains, leading to faster chain relaxation and partial disruption of the matrix structure. As a result, the encapsulated ACN molecules can more easily diffuse through the swollen network, thereby enhancing

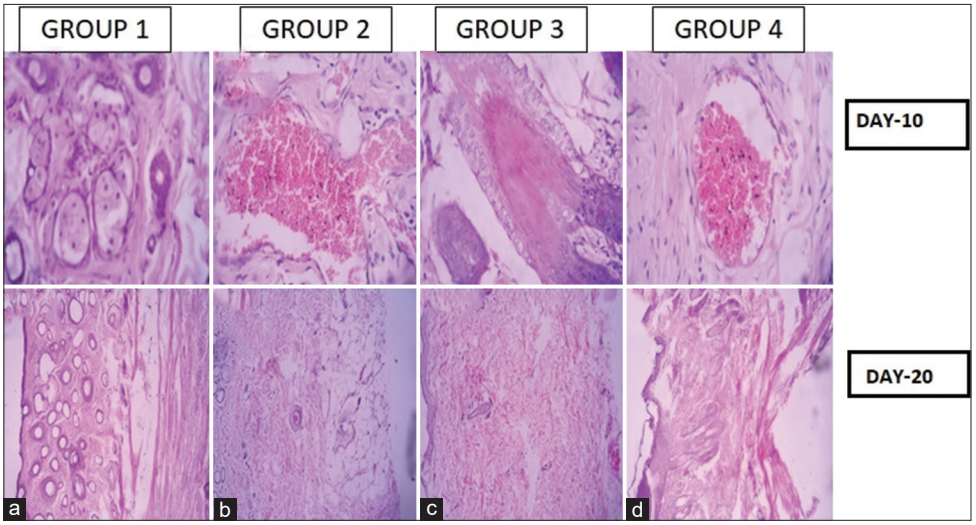

Fig. 11: (a-d) Represents the histological image of Group 1 (Control), Group 2 (Stress-induced), Group 3 (Standard treatment), Group 4 (Test-1) (nanofiber formulation containing the drug anthocyanin)

their release rate from the polymer system. The release data fitted best to the Korsmeyer–Peppas model, indicating a non-Fickian (anomalous) diffusion mechanism**.** This suggests that ACN release from the PVA–SS matrix occurs through a combined process of diffusion and polymer relaxation or degradation, facilitated by the hydrophilic and swelling nature of sericin. The cumulative drug release data across various wavelengths were analyzed to determine the release kinetics. The presence of aromatic amino acids such as phenylalanine, tryptophan, and tyrosine, which correlate to an absorption peak at 276 nm, indicates that sericin is present in the phytoconstituents.

Wound healing activity study

When the skin is injured, fluid leaks from damaged blood and lymphatic vessels, a process counteracted by hemostasis. Platelets aggregate at the wound site, forming a clot that seals the defect while secreting growth factors to aid in the healing process. Subsequently, chemokines released by platelets activate inflammatory cells, triggering the onset of the inflammatory phase. The release of growth factors and cytokines during this phase causes macrophages and other immune cells to go toward the wound, where they eliminate cell debris and fight off invasive microorganisms. The process of re-epithelialization ultimately starts with keratinocyte proliferation. In the proliferation phase, fibroblasts change into myofibroblasts, which promote the development of granulation tissue. At the same time, the myofibroblasts break down and reorganize the ECM.

In Fig. 10 nad Table 4 represents over time, the wound size progressively reduced. The controlled rat displayed the slowest healing wound closure rates (Control) with drug and polymer samples containing different concentration wound closure rates of (ACN 0.1%) and (ACN 1%) on the 1st day, 0%, respectively. The rats treated with the combination of both drug and polymer nanofiber showed better healing, with closure rates of 42.3±3.1% (Control), 56.8±4.0% (ACN 0.1%), and 68.2±3.5% (ACN 1%) on the 14th day. However, the rat treated with nanofiber containing both drug and polymer exhibited the most significant healing, achieving 65.7±4.5%, 82.5±3.8%, and 92.4±2.7% closure on 21 days. These findings indicate that the developed nanofiber effectively promotes wound healing by stimulating and accelerating wound closure. One-way ANOVA showed significant differences in wound contraction among groups at day-14 ($p<0.05$) and day-21 ($p<0.01$).

Histopathology study

Histological analysis was carried out on skin tissues collected from all six experimental groups on day-10 and day-20 to assess the extent of wound healing and tissue regeneration. Fig. 11 displayed the Group 1 (Control), on both day-10 and day-20, the skin sections showed normal histoarchitecture with intact epidermis and dermis, serving as the baseline reference. The Group 2 (stress-induced) showed marked pathological changes. Day-10 sections revealed disrupted epidermal integrity, edema, inflammatory infiltration, and dermal degeneration. These features persisted on day-20, with signs of chronic inflammation and incomplete re-epithelialization. The Group 3 (Standard treatment) showed considerable wound healing. By day-10, mild inflammatory cell infiltration and early stages of re-epithelialization were evident. By day-20, tissue architecture appeared nearly restored, closely resembling the control group. Group 4 (Test-1) (nanofiber formulation containing drug ACN) demonstrated effective healing. On day-10, moderate epithelial regeneration and reduced inflammatory response were seen. By day-20, the tissue exhibited nearly complete re-epithelialization, collagen deposition, and restoration of dermal structure, comparable to the standard group.

CONCLUSION

The research underscores the encouraging potential of ACN-infused PVA and SS nanofiber dressings in improving wound healing for injured patients, owing to their potent antibacterial properties and notable anti-inflammatory effects. The optimal formulation exhibited excellent fluid absorption and a controlled release of the herbal phytoconstituents, resulting in impressive healing rates. This indicates a promising and innovative strategy for wound care in individual patients. The intricate processes of wound healing encompass various phases characterized by fibroblast proliferation, ECM deposition, and neovascularization, all of which are essential for effective tissue regeneration and repair. The observed histopathological changes not only reflect the dynamic nature of healing but also underscore the importance of understanding these mechanisms to enhance therapeutic interventions in wound management.

ACKNOWLEDGMENT

We would like to thank the School of Pharmaceutical Sciences, Siksha 'O' Anusandhan (Deemed to be a university), Bhubaneswar, Odisha, for offering the various facilities I used for my research work.

AUTHOR'S CONTRIBUTIONS

Jajnadatta Panda is credited with designing, data acquisition, analysis, interpretation, drafting, and revision of the script. Dr. Pritipadma Panda and Archana Panigrahy are credited with the analysis and revision of the script. Dr. Abhisek Pal aided with supervision, conceptualization, interpretation, and analysis.

ETHICAL STATEMENT

This material is the author's original work, which has not been previously published elsewhere. The paper reflects the author's research and analysis truthfully and completely. The results are appropriately placed in the context of prior and existing research. The paper properly credits the meaningful contributions of co-authors and co-researchers. The research ethics committee of SOA (Deemed to be University), School of Pharmaceutical Sciences, approved the animal treatment protocol under Approval No: IAEC/SPS/SOA/181/2024.

CONFLICT OF INTEREST

No potential conflict of interest was reported by the authors.

FUNDING

The author(s) received no financial support for the research, authorship, and/or publication of this article.

REFERENCES

1. Andrades U, Gaikar S, Nathani K, Sawarkar S, Omri A. Harnessing nanofibers for targeted delivery of phytoconstituents in age-related macular degeneration. Drug Deliv. 2025;32(1):2489491. doi: 10.1080/10717544.2025.2489491, PMID 40192800
2. Badekar R, Bodke V, Tekade BW, Phalak SD. An overview on oral thin films-methodology, characterization and current approach. Int J Pharm Pharm Sci. 2024;16(4):1-10. doi: 10.22159/ijpps.2024v16i4.50386
3. Abdelazim EB, Abed T, Goher SS, Alya SH, El-Nashar HA, El-Moslamy SH, *et al*. *In vitro* and *in vivo* studies of *Syzygium cumini*-loaded electrospun PLGA/PMMA/collagen nanofibers for accelerating topical wound healing. RSC Adv. 2024;14(1):101-17. doi: 10.1039/d3ra06355k, PMID 38173621
4. Cho YS, Yoon H, Jin SG. Novel *Saccharomyces cerevisiae*-loaded polyvinyl pyrrolidone/SiO_2 nanofiber for wound dressing prepared using electrospinning method. Materials (Basel). 2024;17(12):2903. doi: 10.3390/ma17122903, PMID 38930272
5. Mohammadi G, Safari M, Karimi M, Iranpanah A, Farzaei MH, Fakhri S, *et al*. Preparation and characterization of *Pistacia atlantica* oleo-gum-resin-loaded electrospun nanofibers and evaluating its wound healing activity in two rat models of skin scar and burn wound. Front Pharmacol. 2024;15:1474981. doi: 10.3389/fphar.2024.1474981, PMID 39654617
6. Amer AA, Mohammed RS, Hussein Y, Ali AS, Khalil AA. Development of *Lepidium sativum* extracts/PVA electrospun nanofibers as wound healing dressing. ACS Omega. 2022;7(24):20683-95. doi: 10.1021/acsomega.2c00912, PMID 35755335
7. Sukum P, Punyodom W, Dangtip S, Poramapijitwat P, Daranarong D, Jenvoraphot T, *et al*. Argon plasma jet-treated poly (vinyl alcohol)/chitosan and PEG 400 plus *Mangifera indica* Leaf extract for electrospun nanofiber membranes: *In vitro* study. Polymers (Basel). 2023;15(11):2559. doi: 10.3390/polym15112559, PMID 37299357
8. Mary SA, Ariram N, Gopinath A, Chinnaiyan SK, Raja IS, Sahu B, *et al*. Investigation on centrifugally spun fibrous PCL/3-methyl mannoside mats for wound healing application. Polymers (Basel). 2023;15(5):1293. doi: 10.3390/polym15051293, PMID 36904532
9. Mouro C, Gomes AP, Ahonen M, Fangueiro R, Gouveia IC. *Chelidoniummajus* L. Incorporated emulsion electrospun PCL/PVA_PEC nanofibrous meshes for antibacterial wound dressing applications. Nanomaterials (Basel). 2021;11(7):1785. doi: 10.3390/nano11071785, PMID 34361171
10. Samokhin Y, Varava Y, Diedkova K, Yanko I, Husak Y, Radwan-Pragłowska J, *et al*. Fabrication and characterization of electrospun chitosan/polylactic acid (CH/PLA) nanofiber scaffolds for biomedical application. J Funct Biomater. 2023;14(8):414. doi: 10.3390/jfb14080414, PMID 37623659
11. Elhabal SF, Al-Zuhairy SA, El-Nabarawi M, Mohamed Elrefai MF, Shoela MS, Hababeh S, *et al*. Enhancing photothermal therapy for antibiofilm wound healing: Insights from graphene oxide-cranberry nanosheet loaded hydrogel *in vitro*, *in silico*, and *in vivo* evaluation. Int J Nanomedicine. 2024;19:12999-3027. doi: 10.2147/IJN.S482836, PMID 39651355
12. Li H, Chen X, Lu W, Wang J, Xu Y, Guo Y. Application of electrospinning in antibacterial field. Nanomaterials (Basel). 2021;11(7):1822. doi: 10.3390/nano11071822, PMID 34361208
13. Moharram BA, Al-mahbashi HM, Al-maqtari T, Saif-ali R, A-doaiss AA. Aloe irafensis an endemic plant of Yemen: Phytochemical screening, antibacterial, antioxidant, and wound-healing activities. Asian J Pharm Clin Res. 2021 Oct 14(10):88-94. doi: 10.22159/ajpcr.2021.v14i10.41832
14. Qadir A, Jahan S, Aqil M, Warsi MH, Alhakamy NA, Alfaleh MA, *et al*. Phytochemical-based nano-pharmacotherapeutics for management of burn wound healing. Gels. 2021;7(4):209. doi: 10.3390/gels7040209, PMID 34842674
15. Li Y, Tan Y, Zhao H, Chen S, Nilghaz A, Cao R, *et al*. Green biosynthetic silver nanoparticles from *Ageratum conyzoides* as multifunctional hemostatic agents: Combining hemostasis, antibacterial, and anti-inflammatory properties for effective wound healing. Mater Today Bio. 2025;31:101468. doi: 10.1016/j.mtbio.2025.101468, PMID 39906203
16. Ponphaiboon J, Krongrawa W, Aung WW, Chinatangkul N, Limmatvapirat S, Limmatvapirat C. Advances in natural product extraction techniques, electrospun fiber fabrication, and the integration of experimental design: A comprehensive review. Molecules. 2023;28(13):5163. doi: 10.3390/molecules28135163, PMID 37446825
17. Jia X, Dou Z, Zhang Y, Yu C, Yang M, Xie H, *et al*. Application of a novel thermal/pH-responsive antibacterial paeoniflorin hydrogel crosslinked with amino acids for accelerated diabetic foot ulcers healing. Mater Today Bio. 2025;32:101736. doi: 10.1016/j.mtbio.2025.101736, PMID 40255581
18. Kasinathan ID, Manivannan K, Ramasamy M. Traditionally used medicinal plants for wound healing in Thiruvallur district, Tamil Nadu, India. Int J Curr Pharm Res. 2024 Jul;16(4):1-6. doi: 10.22159/ijcpr.2024v16i4.4086
19. Atiyah R, Al-edresi S. Preparation and justification of nanofibres-loaded mafenide using electrospinning technique to control release. Int J Appl Pharm. 2024;16(2):224-30. doi: 10.22159/ijap.2024v16i2.49691
20. Valentina Y, Pandian J. A novel wound dressing with silkworm cocoon scaffold to fasten wound healing: An *in vivo* study using rat excision wound model. Asian J Pharm Clin Res. 2024;17(10):30-4. doi: 10.22159/ajpcr.2024v17i10.52201
21. Trabelsi M, Mamun A, Klöcker M, Moulefera I, Pljonkin A, Elleuch K, *et al*. Magnetic carbon nanofiber mats for prospective single photon avalanche diode (SPAD) sensing applications. Sensors (Basel). 2021;21(23):7873. doi: 10.3390/s21237873, PMID 34883875
22. Mirzaeei S, Taghe S, Asare-Addo K, Nokhodchi A. Polyvinyl alcohol/chitosan single-layered and polyvinyl alcohol/chitosan/Eudragit RL100 multi-layered electrospun nanofibers as an ocular matrix for the controlled release of ofloxacin: An *in vitro* and *in vivo* evaluation. AAPS PharmSciTech. 2021;22(5):170. doi: 10.1208/s12249-021-02051-5, PMID 34085150
23. Serag E, El-Aziz AM, El-Maghraby A, Taha NA. Electrospun non-wovens potential wound dressing material based on polyacrylonitrile/chicken feathers keratin nanofiber. Sci Rep. 2022;12(1):15460. doi: 10.1038/s41598-022-19390-3, PMID 36104428
24. Kanaujiya S, Arya DK, Pandey P, Singh S, Pandey G, Anjum S, *et al*. Resveratrol-ampicillin dual-drug loaded polyvinylpyrrolidone/polyvinyl alcohol biomimic electrospun nanofiber enriched with collagen for efficient burn wound repair. Int J Nanomedicine. 2024;19:5397-418. doi: 10.2147/IJN.S464046, PMID 38863647